# Shaking table tests of lightly RC walls: Numerical simulations

N. Ile, X. H. Nguyen, Panagiotis Kotronis, J. Mazars, J. M. Reynouard

# Shaking Table Tests of Lightly RC Walls: Numerical Simulations

NICOLAE ILE[1], XUAN-HUY NGUYEN[2], PANAGIOTIS KOTRONIS[2], JACKY MAZARS[2], and JEAN MARIE REYNOUARD[1]

[1]LGCIE INSA Lyon, Bâtiment Coulomb, Villeurbanne, France
[2]Laboratoire Sols, Solides, Structures-Risques (3S-R), UJF/INPG/CNRS, Grenoble, France

*In the framework of the European consortium ECOLEADER, a seismic research project has been performed on specimens tested on a shaking table. The specimens were representative of reinforced concrete buildings with bearing walls. The mock-up studied in particular in this article is composed of two parallel walls linked with a perpendicular one that has openings. The walls are reinforced according to the current design practice in France with a small amount of reinforcement. Two kinds of finite element simulations have been performed: a refined one using a detailed 3D description of the specimen and a simplified one, based on multifiber beams. The comparison between the experimental and numerical results not only demonstrates the accuracy of the time-history analysis models, but also allows obtaining more detailed information about the behavior of the specimen for more complex seismic excitations. It is shown that both models are able to describe quantitatively the global and qualitatively the local behavior of the structure. The simplified model is furthermore used to investigate the behavior of the specimen under a 3D earthquake loading.*

**Keywords** Wall; Multifiber Beam; Shaking Table; Concrete

## 1. Introduction

Many European buildings are situated in seismic regions of low or moderate seismicity. Among these, a large part is not designed following modern seismic design codes. It is thus evident that the evaluation of the vulnerability of existing structures is a crucial issue. In the framework of ECOLEADER (European Consortium of Laboratories for Earthquake and Dynamic Experimental Research), a seismic research project has been recently performed with specimens tested dynamically on a shaking table. The mock-ups are representative of reinforced concrete buildings with longitudinal and transverse bearing walls, such as built in the 1960's and later in great number in many European countries. More specifically, the project deals with two structures: a Slovenian and a French one. The first one was designed according to the current practice in Eastern European Countries, the second one according to the French design code PS 92. All the tests have been performed on the large shaking table located at the Laboratório Nacional de Engenharia Civil (LNEC) in Lisbon, Portugal.

The work presented in this article is related to the numerical simulations and analysis of the response of the French specimen [Kotronis, *et al.*, 2005b; Mazars *et al.*, 2005;

Address correspondence to Panagiotis Kotronis, Laboratoire Sols, Solides, Structures-Risques (3S-R), UJF/INPG/CNRS and RNVO, Domaine Universitaire BP 53, 38041 Grenoble Cedex 9, France; E-mail: panagiotis.kotronis@inpg.fr

Bisch and Coin, 2005; Nguyen, 2006; Nguyen *et al.*, 2006]. It is a multi-story building cell composed of two parallel lightly reinforced concrete (RC) walls braced with a third wall with openings. All the walls are designed for the seismic level prescribed for a typical seismic region in France. Two orthogonal directions of loading (accelerograms) are considered. During each test, global and local measurements are made in order to study the behavior of the specimen (displacements, accelerations, strains, crack openings, etc.).

The objective of this work is to verify the design assumptions and obtain more detailed information about the behavior of walls with limited reinforcement when subjected to more complex loading conditions, information that the experimental program was unable to provide. This article emphasizes some particular aspects of the behavior of the ECOLEADER specimen and then compares test results with numerical predictions based on two different modeling strategies: a refined one using a 3D finite element description and a simplified one based on a multifibre beam approach. This comparison helps to verify the numerical models and to better understand the global and local behavior of the test specimen.

It is shown that both models are able to describe the global behavior of the structure and qualitatively the local phenomena. The results confirm once again the conclusions of previous works done in France about the good behavior of lightly RC walls in seismic regions of low or moderate seismicity [Bisch and Coin, 1994, 1998, 2002; Mazars, 1998; Sollogoub *et al.*, 2000; Combescure *et al.*, 2002; Ile *et al.*, 2002; Ile and Reynouard, 2003; Kotronis *et al.*, 2005c]. The simplified model is finally used to investigate the influence of a 3D earthquake loading.

In the section that follows, a brief summary of the design background is provided in order to familiarize the reader with the ECOLEADER program.

## 2. Design of the Test Specimen

The design and construction method of RC-bearing walls in France often differ from the usual practice in other countries. Mainly for architectural reasons, a building contains usually an important number of lengthy RC walls disposed in two directions that bear a great part of the vertical load. It is difficult to imagine such walls designed according to the classical capacity design procedure privileging the development of a plastic hinge at the base, while the upper part of the wall is over reinforced to remain elastic. The French design philosophy instead—recently also adopted in the Eurocode 8 for such type of buildings—opts for a distribution of the flexural reinforcement in accordance with the bending moment diagram. In this way, damage may develop throughout the height of the building and not only at the base.

The specimen is designed according to the European regulation EC8-1 with the French appendix (PS92, 1995; Eurocode 8, 1995, 2004). It is a five story building cell composed of two parallel RC walls braced with a third wall with openings. The walls are connected to six square concrete slabs; see Fig. 1. The following design rules have been followed [Bisch and Coin, 2005, 2006, 2007; Coin and Bisch, 2005; Bisch *et al.*, 2007].

Considerations of symmetry (in order to separate the phenomena and to simplify the analysis of the results), of maximum weight supported by the table, of weight and congestion of the additional masses, of a sufficient number of levels to obtain a significant slenderness of the walls, of the dimensions to be respected for easy fixings on the table, and of the similitude rules related to the conservation of acceleration, led to a similitude ratio of 1/3 for lengths, which also led naturally to all the other choices [Bisch and Coin, 2005]:

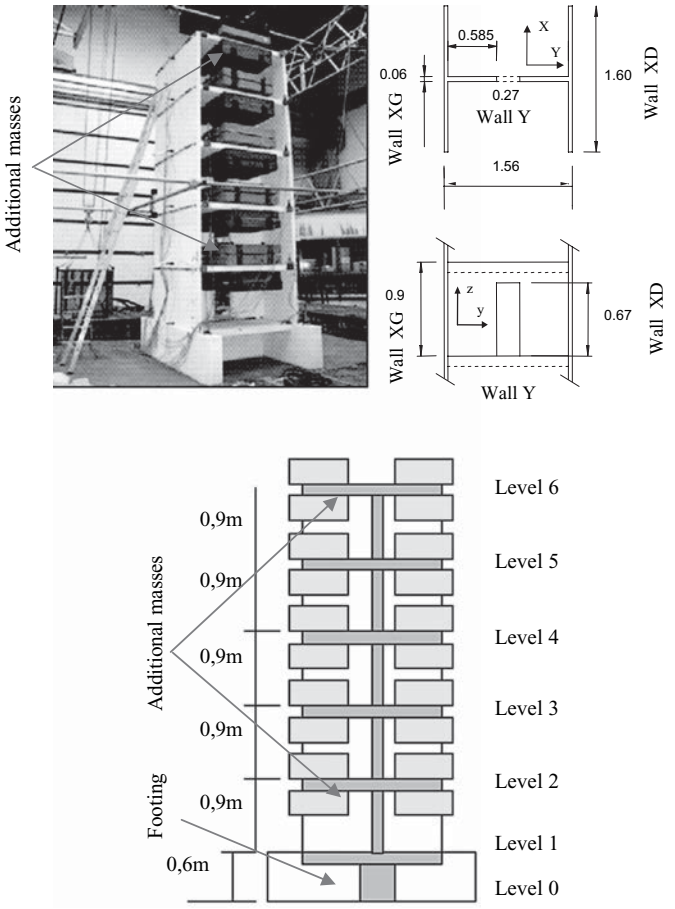


**FIGURE 1** Geometrical data of the specimen (m).

- The length of a wall (usually approximately 5 m) is taken equal to 1.6 m.
- The thickness of a wall (usually 18 cm) is taken equal to 6 cm.
- The height of each story (usually 2.7 m) is taken equal to 0.9 m. The total height of the specimen is 5.1 m.
- The width of the slabs of each story (usually 18–20 cm) is taken equal to 8 cm.
- By assumption, stresses are preserved. In order to have realistic normal stresses due to the gravity forces at the bottom of the specimen, additional masses are used (Fig. 1, Table 1). The total mass is about 5,200 kg (specimen) + 24,000 kg (additional masses) + 2,400 kg (footing) = 31,600 kg. The axial stress at the base of the walls is 1.1 MPa. This value is between the stress of an intermediate wall (1.39 MPa) and of a façade wall (0.88 MPa) of a real building.
- Consequently, accelerations are preserved.
- Time is divided by $\sqrt{3} = 1.732$.
- The ordinates of the design spectrum are preserved, whereas the periods as a variable of the spectrum are reduced in the same way as time.
- Relative eccentricities are preserved.

**TABLE 1** Distribution of masses

| Level | Height | Above/Below the slab | Wall XG (Wall XD) | Wall Y | Total Masses |
|---|---|---|---|---|---|
| 6 | 5.06 m | Above | 0 | 0 | 0 |
| | | Below | 1906.1 kg | 1467.8 kg | 5280 kg |
| 5 | 4.16 m | Above | 2093.6 kg | 1612.4 kg | 5800 kg |
| | | Below | 3999.9 kg | 3080.2 kg | 11080 kg |
| 4 | 3.26 m | Above | 4187.6 kg | 3224.8 kg | 11600 kg |
| | | Below | 6093.7 kg | 4692.6 kg | 16880 kg |
| 3 | 2.36 m | Above | 6281.4 kg | 4837.2 kg | 17400 kg |
| | | Below | 8187.5 kg | 6305 kg | 22680 kg |
| 2 | 1.46 m | Above | 8375.2 kg | 6449.6 kg | 23200 kg |
| | | Below | 10281.3 kg | 7917.4 kg | 28480 kg |
| 1 | 0.56 m | Above | 10469 kg | 8062 kg | 29000 kg |
| | | Below | | | 29480 kg |
| 0 | 0 | Above | | | 31200 kg |
| | | Below | | | 31600 kg |

The fundamental periods of the specimen are calculated in both directions X and Y using the classical Rayleigh method [Chopra, 2000]. The design spectrum provides the acceleration $S$ to apply to the structure.

According to Bisch and Coin [2007], the spectral accelerations being preserved, the level of seismic loading applied to the specimen during the shaking table tests is, in theory, that to which a real building could be subjected in a given area. If in the real building the bracing walls carry only one part of the loads (the remainders being carried for example by columns of much lower stiffness), then the embarked mass (the portion of mass that gives place to the seismic forces due to the effect of the action of the seismic acceleration) is larger than the carried mass (the mass which generates the vertical load). As the two masses (carried and embarked) are equal in the case of the present experiment, it is necessary to increase the seismic acceleration in the same ratio than that of the embarked mass to the carried mass of the real building, to obtain an equivalent level of loading. More specifically, we have the following:

To represent the current architectural situation in France, the ratio between the two masses was fixed to 2 in the X direction, so that when the specimen is subjected to a certain level of acceleration on the table, half of it represents the corresponding acceleration applied to the real building (the frequency remaining on the plateau of the spectrum, this does not modify the spectral response). The ratio between the two masses was fixed to 1 in the Y direction. The model was designed for an acceleration equal to 0,50 g at the level of the table, in the X direction, and of 0,25 g in the Y direction. This corresponds to a peak ground acceleration of 0,25 g in both directions for the real building [Bisch and Coin, 2005]; the fundamental periods of such lightly RC walls structures being inferior to the limit period $T_C$ of the design spectrum, one can express the design values in terms of peak ground accelerations rather that in terms of spectral coordinates.

The behavior factor $q$ (also known as reduction factor, used to reduce design forces in earthquake resistant design) is chosen using a stain energy criterion [PS92, 1995; Bisch and Coin, 2006]. It is checked that the strain energy calculated considering realistic

reinforced concrete behavior is at least equal to that obtained using an elastic behavior. The method is as follows:

- The shear force $F_t$ at the base of the specimen and the corresponding displacement $d_e$ are calculated using an elastic model (Fig. 2).
- An equivalent behavior factor $q$ is chosen.
- The new shear force $F_b$ is calculated as $F_b = F_t / q$.
- Deformations are calculated using the classical reinforced concrete theory. One can then deduce the displacements and the capacity curve corresponding to an ultimate displacement $d_{ul}$.
- The value of the behavior factor $q$ is acceptable if the areas of the surfaces calculated using the elastic model and the classical reinforced concrete theory are the same.

It is to be noted that the design method used in the French standard PS92 [PS92, 1995] is similar to a displacement based approach, with additional conditions regarding the equivalence of energy. This design method leads to a behavior factor $q = 3.5$ for the wall specimen. According to the French design code PS92, in order to prevent shear failure and in recognition of the fact that the behavior factor corresponding to shear is not the same as in pure flexure, design shear forces are increased to about twice the seismic shear forces derived from the analysis. This is taken into account by multiplying the shear force obtained from analysis by the factor $q' = (q+1)/2$.

The reasons for this magnification of the shear force are [Bisch and Coin, 2007]:

- Capacity design makes it possible to avoid brittle failures due to shear or slip and to thus support the emergence of the cracking due to flexure. It results in resisting a shear force at least equal to that which would result from the simple balance when the resisting moment is reached, by taking into account a suitable overstrength factor to the resisting moment. The overstrength factor depends in particular on the hardening of steel bars and is considered as being about 1.3.
- Time history simulations on models, taking into account the actual behavior of reinforced concrete, have shown that the reduction of the seismic action effects

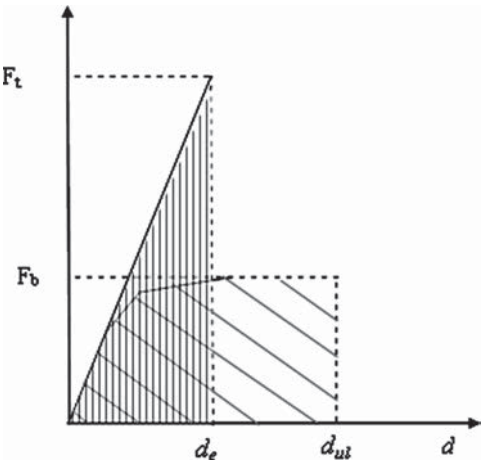


**FIGURE 2** Strain energy criterion for calculating the equivalent behavior factor.

when compared to the effects obtained in the elastic assumption is not the same for all actions. Particularly, it differs between bending moments and shear forces.

With the behavior factor known, the forces and the reinforcement can be calculated. In the X direction, the main reinforcement is determined by the bending moment with the axial force and it is just adapted to fit with the strength demand. For the wall in the Y direction forces and moments in the piers and the lintels are balanced in a lattice model [Bisch and Coin, 2005]. Shear reinforcement was found to be needed only for the Y wall and the lintels. The reinforcement used is presented in Fig. 3 and Table 2. More precisely:

- Vertical reinforcement is not distributed uniformly in the walls but concentrated at the following specific areas: the four angles of the specimen, the two joints between the X walls with the Y wall, the left and right side of the opening situated in the Y wall.

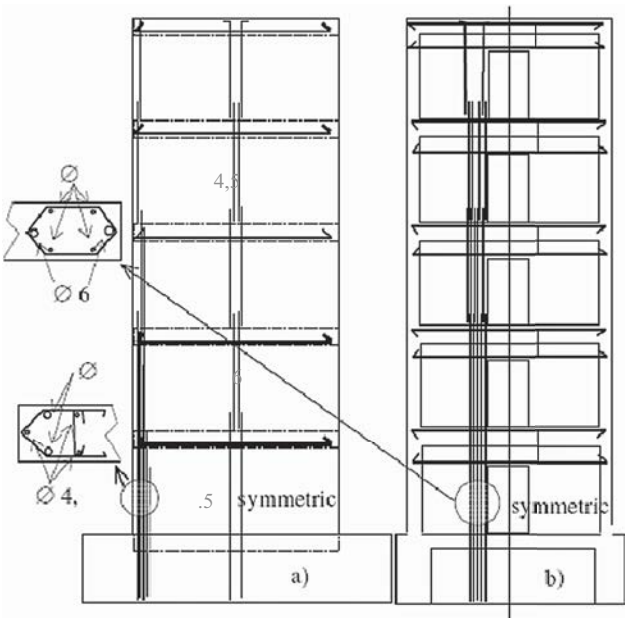


**FIGURE 3** Reinforcement: (a) Walls in the X direction; (b) Wall and lintels in the Y direction [Bisch and Coin, 2005].

**TABLE 2** Reinforcement

| Level | Vertical reinforcement Y wall | Vertical reinforcement X wall | Vertical ties at the crossing of two walls |
|---|---|---|---|
| 5–6 | 2 Φ6 = 0.57 $cm^2$ | 1 Φ4.5 = 0.159 $cm^2$ | 2 Φ4.5 = 0.318 $cm^2$ |
| 4–5 | 2 Φ4.5 + 2 Φ6 = 0.88 $cm^2$ | 1 Φ4.5 = 0.159 $cm^2$ | 2 Φ4.5 = 0.318 $cm^2$ |
| 3–4 | 3 Φ4.5 + 2 Φ6 = 1.04 $cm^2$ | 2 Φ4.5 = 0.318 $cm^2$ | 2 Φ4.5 = 0.318 $cm^2$ |
| 2–3 | 4 Φ4.5 + 2 Φ6 = 1.20 $cm^2$ | 2 Φ5 + 1 Φ4.5 = 0.561 $cm^2$ | 2 Φ4.5 = 0.318 $cm^2$ |
| 1–2 | 4 Φ4.5 + 2 Φ6 = 1.20 $cm^2$ | 2 Φ5 + 3 Φ4.5 = 0.869 $cm^2$ | 2 Φ4.5 = 0.318 $cm^2$ |

- The spacing of the stirrups is 4.5 cm.
- The ratios of the vertical reinforcement (steel section/concrete section) vary from 0.38% at the base of the first level to 0.09% at the base of the 5$^{th}$ level.

Detailed plans of the reinforcement can be found in [Coin and Bisch, 2005; Nguyen, 2006; Bisch *et al.*, 2007].

## 3. Experimental Program and Experimental Results

Two orthogonal directions of loading were applied: X (parallel to the main walls) and Y (parallel to the wall connecting the main ones). The input signals have been derived from two EC8-1-1 spectra, soil type B, corresponding to the Tolmezzo earthquake (Tolmezzo N-S for the X direction and Tolmezzo E-W for the Y direction).

Generated accelerograms at different levels have been used (PGA = from 0.3–0.85 g for direction X and from 0.14–0.50 g for direction Y).

The different sequences are presented in Fig. 4 and Table 3 (T3 level corresponds approximately to the design level). The apparent mode has been measured after each test to follow the evolution of stiffness. Various data have been collected from the different tests: strains on steel bars, displacements, accelerations, etc. Detailed information on the experimental program and results can be found in Bisch and Coin [2005], Mazars *et al.* [2005], Nguyen [2006], and Bisch *et al.* [2007]. An outline of the experimental behavior of the specimen follows:

Cracks developed gradually in the walls and became significant at the design level T3. At this level, horizontal cracks opened at the base of the X walls. At each edge of these walls, reinforcement bars buckled and the concrete was locally crushed (Fig. 5). One of the buckled reinforcement bars was broken. Fine cracks were also developed at the Y wall (Fig. 6). Beyond the design level, the edges of the walls degraded gradually but the previously buckled bars did not break (Fig. 7). During the last test, many reinforcement bars were finally broken, however the mock up continued to resist with an overall rocking mechanism (Fig. 8) [Bisch and Coin, 2005]. Buckling of the reinforcement bars at the design level T3 was unexpected, as it is not a failure mode predicted by the design philosophy adopted. However, this local failure did not influence significantly the performance of the specimen, which was able to resist to much more important levels of loading (until level T6).

## 4. Modeling Strategies

Two finite element simulation strategies have been performed to reproduce the non linear behavior of the specimen: a refined one using a detailed 3D description of the specimen and a simplified one, based on multifibre beams. Taking advantage of the ability of the computer codes to save the accumulated damage state at the end of each analysis, the input motions applied during the experiment were considered in chronological order. Details of the models that were selected for this study are given below:

### *4.1. Refined Model*

The numerical analyses have been performed using the general purpose finite element program CAST3M developed at CEA Saclay, France (Cast3M). To predict the inelastic seismic response with sufficient accuracy, due care has been given to create a detailed model of the specimen, taking into account the necessary geometric characteristics,

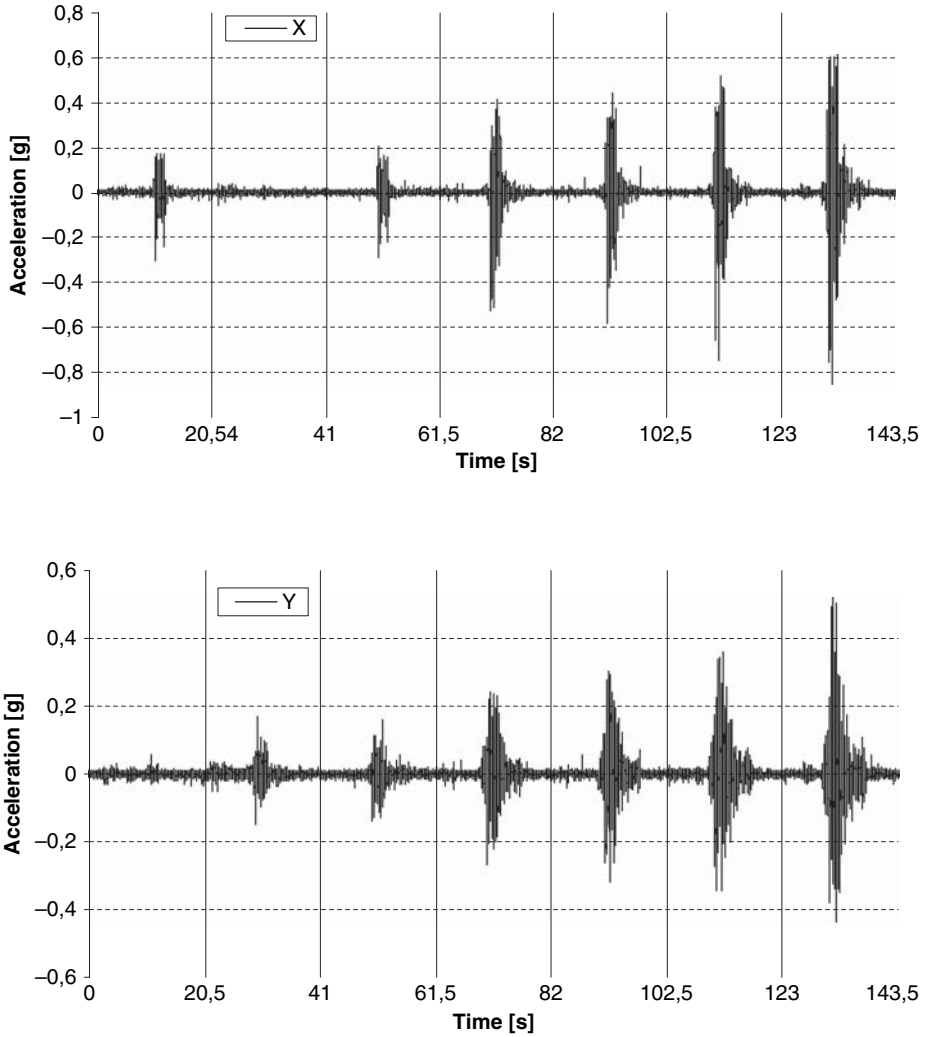


**FIGURE 4** Sequences of the tests.

**TABLE 3** Experimental program

| Stages | Direction X | Direction Y |
|---|---|---|
| T0 | 0.3g | – |
| T1 | – | 0.14g |
| T2 | 0.24g | 0.13g |
| T3 | 0.45g | 0.27g |
| T4 | 0.55g | 0.30g |
| T5 | 0.74g | 0.36g |
| T6 | 0.85g | 0.50g |


**FIGURE 5** State of the XD wall at the design level T3.

**FIGURE 6** State of the Y wall at the design level T3.

construction details and boundary conditions. Since in-plane as well as out-of-plane behavior of the walls need to be analyzed, layered thin shell discrete Kirchoff triangles (DKT) are used to represent the two walls and the slabs. A discrete modeling is adopted to represent the reinforcement through the use of two-node truss-bar elements and perfect bond was assumed to exist between concrete and reinforcement. An example of the 3D finite element mesh used in the analyses is reported in Fig. 9.

During previous tests on CAMUS specimens [Sollogoub *et al.*, 2000; Bisch and Coin, 2002; Kotronis *et al.*, 2005c], it was observed that the specimen oscillation induced vertical and rocking displacements on the shacking table, leading to significant reductions of the corresponding natural frequencies of the whole system (shaking table + specimen). In these conditions, the shaking table itself, in terms of mass and its external supports in terms of stiffness, had to be included into the numerical model. Solid eight-node brick

**FIGURE 7** State of the XD wall at level T5.

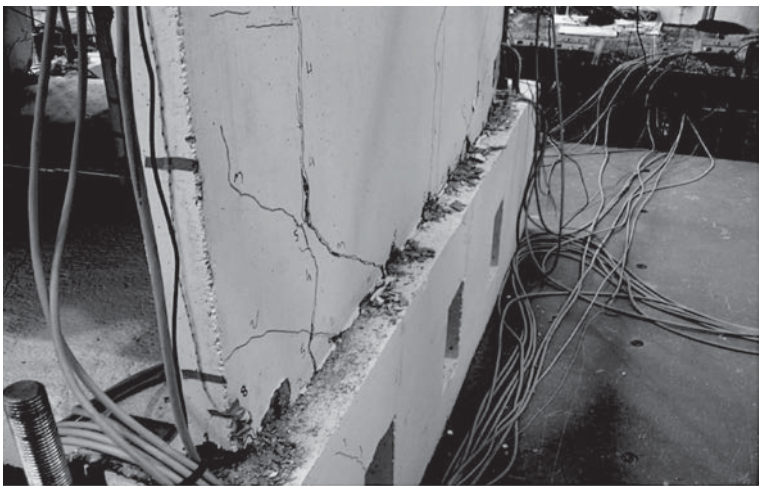

**FIGURE 8** State of the XD wall at the final level T6.

elements are used this time to model the shaking table. Owing to its high stiffness, the finite elements representing the shaking table are assumed to remain elastic and almost infinitely rigid. The total mass of the shaking table (40,000 kg) is uniformly distributed between these finite elements. The vertical and horizontal rods supporting the shaking table are simulated with seven elastic bars, the axial stiffness of each bar being that suggested by the experimenters.

1% critical damping factor (close to the measured damping value) is assumed for the first and second vibration mode. The damping parameters $\alpha$ and $\beta$ are calculated and used subsequently to form the Rayleigh damping matrix $[C] = \alpha[M] + \beta[K]$, $[M]$ and $[K]$ being the mass and stiffness matrix. Despite the fact that a modal characterization is theoretically correct only for linear elastic systems, the damping matrix $[C]$ obtained in this way is assumed to remain constant throughout the loading cycle. To solve the nonlinear equilibrium equations, a modified Newton-Raphson iteration solution scheme is used.

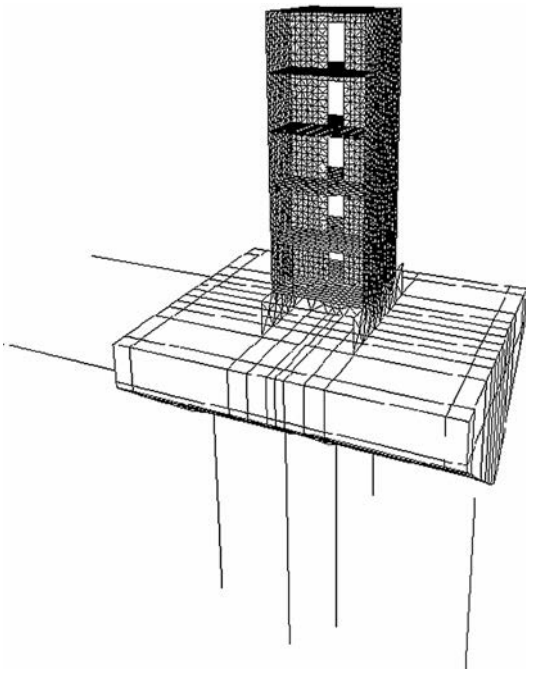

**FIGURE 9** Refined model: finite element mesh.

The behavior of the materials is considered nonlinear, while the foundation is assumed elastic. In order to achieve a good compromise between simplicity and accuracy, a biaxial concrete model providing acceptable representation of the inelastic behavior of concrete under cyclic loading is used [Merabet and Reynouard, 1999]. This model adopts the concept of a smeared crack approach with a possible double cracking only at 90°. It is based upon the plasticity theory for uncracked concrete with isotropic hardening and associated flow rule. Two distinct criteria describe the failure surface: Nadai in compression and bi-compression and Rankine in tension. Hardening is isotropic and an associated flow rule is used. When the ultimate surface is reached in tension, a crack is created perpendicularly to the principal direction of maximum tensile stress. Its orientation is considered fixed. Each direction is then processed independently by a cyclic uniaxial law, while the stress tensor in the local coordinate system (defined by the direction of the cracks) is completed by the shear stress, calculated elastically with a reduced shear modulus $\mu G$ to account for the effect of interface shear transfer ($0 < \mu < 1$, $\mu$ being a function of the crack opening strain).

The behavior of a point initially under tension, which completely cracks prior to undergoing a reverse loading in compression, is illustrated in Fig. 10. Similar laws describe the case of an initially compressed point or of a point that has not totally cracked under a reverse loading. The model has been validated among others using experimental results of shear walls with different span-to-height ratio under monotonic, cyclic and dynamic loading conditions [Ile *et al.*, 2002; Ile and Reynouard, 2000].

To reproduce the nonlinear behavior of the reinforcement, a cyclic model is used that can take into account the Bauschinger effect and the buckling (Fig. 11). The monotonic branch is characterized by an initial linear branch followed by a plateau and hardening up to failure. The cyclic behavior is described by the formulation proposed by Giuffré and

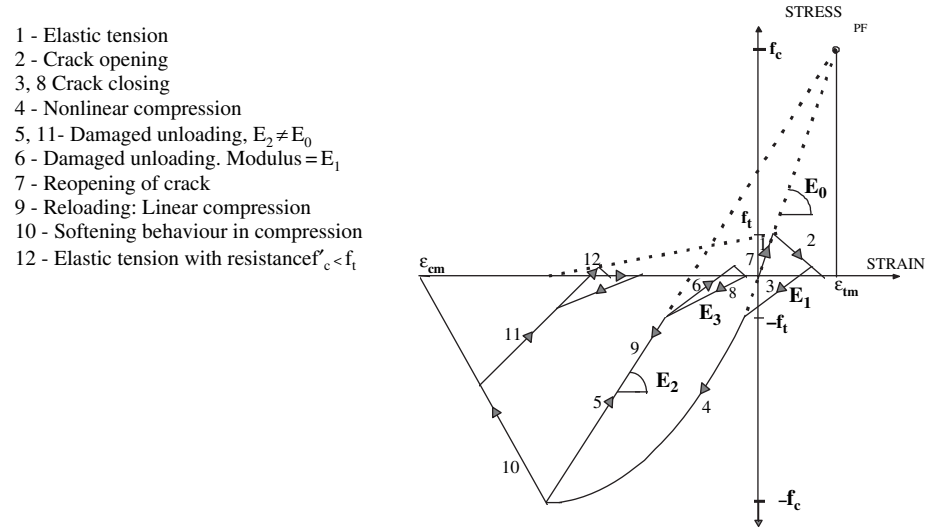


**FIGURE 10** Refined model: uniaxial cyclic law for concrete - point initially in tension.

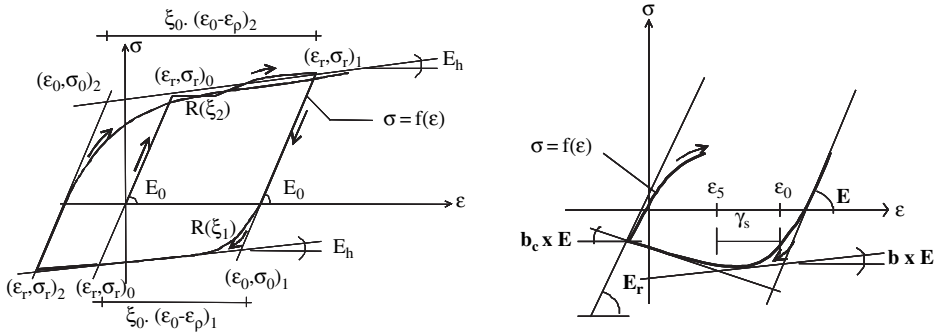


cyclic behavior without buckling

cyclic behavior with buckling

**FIGURE 11** Refined model: uniaxial cyclic law for steel [Guedes *et al.*, 1994].

Pinto and implemented by Menegoto and Pinto [1973]. A detailed description of the steel constitutive law can be found in Guedes *et al.* [1994].

The parameters used for the materials, as provided by the experimental data and the design codes, are: Steel - Elasticity modulus 200,000 MPa, yield stress 660 MPa, failure stress 680 MPa and strain at failure 1.8%. Concrete - Elasticity modulus = 30,000 MPa, compressive strength 32 MPa and tensile strength 2.2 MPa.

### *4.2. Simplified Model*

The necessity to perform parametrical studies and to reduce computational cost led us to adopt the following simplified approach: The specimen is modeled using multifiber beam elements and so the number of degrees of freedom of the mesh is reduced as compared to

the previous approach. The user can define at each fiber a material (in our case concrete or steel) and the appropriate constitutive relation.

Different multifiber beam elements exist in the literature. Timoshenko multifiber beam elements are able to simulate non linear shear but 3D appropriate constitutive relations are needed [Guedes *et al.*, 1994; Combescure and Pegon, 1994; Dubé, 1997; Petrangeli *et al.*, 1999; Kotronis, 2000; Kotronis *et al.*, 2004; Kotronis and Mazars, 2005; Papaioannou *et al.*, 2005; Mazars *et al.*, 2006]. In order to account for nonlinear torsion of a section composed of several materials, a warping-conduction analogy method can be used [Proix *et al.*, 2000; Mazars *et al.*, 2006]. Finally, for cases where nonlinear shear or torsion can be neglected, Euler-Bernoulli multifiber beam elements are appropriate [Taucer *et al.*, 1991; Spacone *et al.*, 1996; Ghavamian and Mazars, 1998; Coleman and Spacone, 2001].

For the following simulations, the Euler Bernoulli multifiber element of the finite element code ASTER is used [Ghavamian *et al.*, 2002; ASTER]. Torsion is considered linear. The finite element mesh is presented in Fig. 12 where multifiber beam of T section have been used to mesh the walls and the horizontal slabs (for a typical RC wall, the number of concrete fibers must at least be such that the quadratic moments of the section are computed accurately by numerical integration. The number and the position of the steel fibers are similar to the number and the position of the actual reinforcement bars. 3 or 4 multifiber elements seem sufficient for each floor. The values of the material parameters in each fiber must be calibrated from experimental results on characteristic specimens). Again, the vertical and horizontal rods supporting the shaking table are simulated with seven elastic bars. The additional masses and the weight load of each floor are concentrated at each story.

The reinforcement steel is modeled using a classical isotropic cinematic law with a linear hardening. The constitutive model for concrete under cyclic loading ought to take into account some observed phenomena, such as decrease in material stiffness due to cracking, stiffness recovery which occurs at crack closure and inelastic strains concomitant to damage. To simulate this behavior, a damage model is adopted having two scalar damage variables, one for damage in tension and one for damage in compression [La Borderie, 1991]. Unilateral effect and stiffness recovery (damage deactivation) are also included. Inelastic strains are taken into account with the aid of an isotropic tensor (Fig. 13). The Rayleigh damping coefficients $\alpha$ and $\beta$ have been adjusted as before to

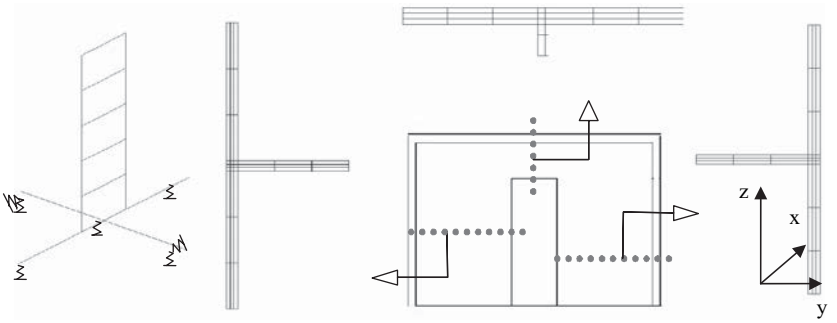


**FIGURE 12** Simplified model: mesh.

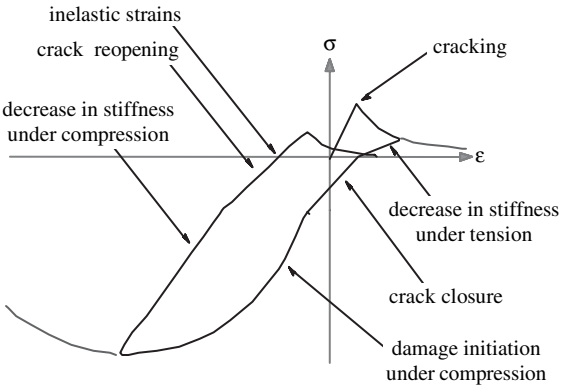


**FIGURE 13** Simplified model: uniaxial response of concrete model for cyclic loading.

ensure a value of 1% for the two first modes. Consistent model parameters with those used in the refined model are adopted.

## 5. Eigenfrequency Analysis

In order to validate the different modeling assumptions, eigenvalue analyses were performed for both finite element models. Elastic material properties were used for the specimen, taking a Young's modulus for concrete equal to 30,000 MPa and 200,000 MPa for steel reinforcement. The stiffness of the springs supporting the shaking table was identified to fit the first three eigenmodes of the shaking table alone (without the specimen), which were known before the tests: 11 Hz, 18 Hz, and 21 Hz.

Table 4 presents the numerical values of the first three natural frequencies of the whole structure (specimen + shaking table) confronted with the test results. The first natural frequency corresponds to the flexural vibration mode in the X direction, while the second natural frequency corresponds to the flexural vibration mode in the Y direction. As shown in the table, the frequency values predicted by the two models agree reasonably well with the measured values. For the torsional mode, unfortunately, no comparison between numerical and experimental results can be made, because the torsional mode was not measured experimentally.

## 6. Nonlinear Transient Dynamic Analysis

Comparison of the numerical time history results with the experimental records is necessary in order to confirm the accuracy of the modeling approaches. Furthermore, numerical results allow to verify design assumptions and to extend the existing limited experimental measurements. More specifically, we have the following:

Evolutions of the bending moments, shear forces, and axial forces during the tests are computed using the absolute accelerations provided by the accelerometers positioned on the specimen and the estimated masses of each floor. Nevertheless, the measurement channels used during the experiments allowed determining with sufficient accuracy only the horizontal (shear) forces, the bending moments in each wall, and the total axial force. The values of the axial internal forces in each wall, which are however important, were not measured. The structure being hyperstatic, theses forces are difficult to evaluate. Since the numerical models provide the individual axial forces in each wall at any

**TABLE 4** Modal analysis

| Strategy | Direction X | Direction Y | Torsion |
|---|---|---|---|
| Simplified model |  |  |  |
| | 4.54 Hz | 7.0 Hz | 11.0 Hz |
| Refined model | 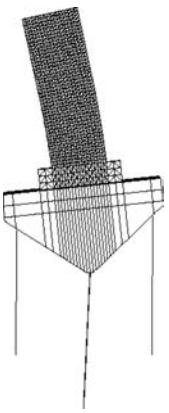 | 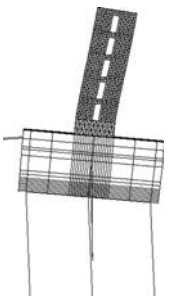 | 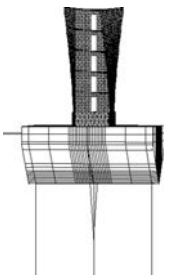 |
| | 4.5 Hz | 7.06 Hz | 9.9 Hz |
| Experiment | 4.5 Hz | 7.13 Hz | not known |

location, their importance in investigating the wall behavior is obvious. In the numerical analysis presented hereafter, all the seismic signals applied during testing (see Table 3) were considered in chronological order. For the sake of brevity, the presentation of the results in the following two sections is not exhaustive but focuses on aspects relevant to the analysis of this wall structure.

### *6.1. Global Results*

The computed and experimental top displacements corresponding to T0 and T1 levels are presented in Figs. 14 and 15. One can see that the behavior in the X direction is correctly predicted by both models (Fig. 14). Peak values (positive and negative) and frequency content are quite similar to the experimental results. Conclusions are quite different in the Y direction. Both models have difficulties to reproduce satisfactorily the experimental behavior of the specimen, although the peak ground acceleration imposed at T1 level is small (0.14 g) and the natural periods have already been calibrated with the experimental ones (Table 4). Naturally, differences are more important in the case of the simplified model.

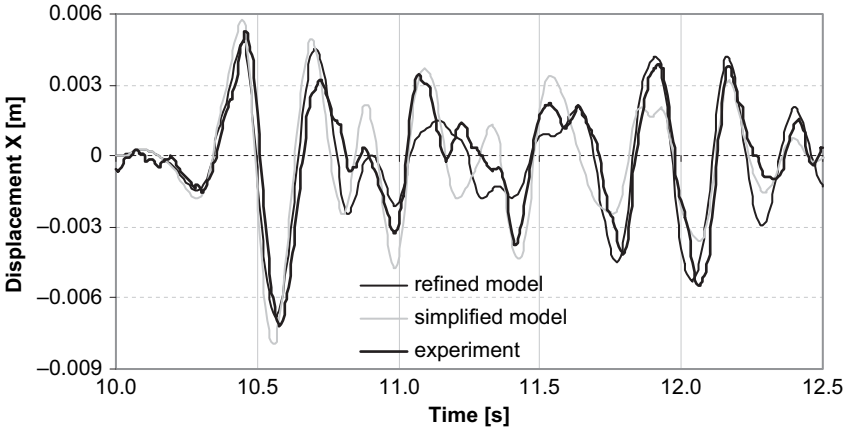


**FIGURE 14** Calculated and measured horizontal relative top X displacement for the two models - Level T0.

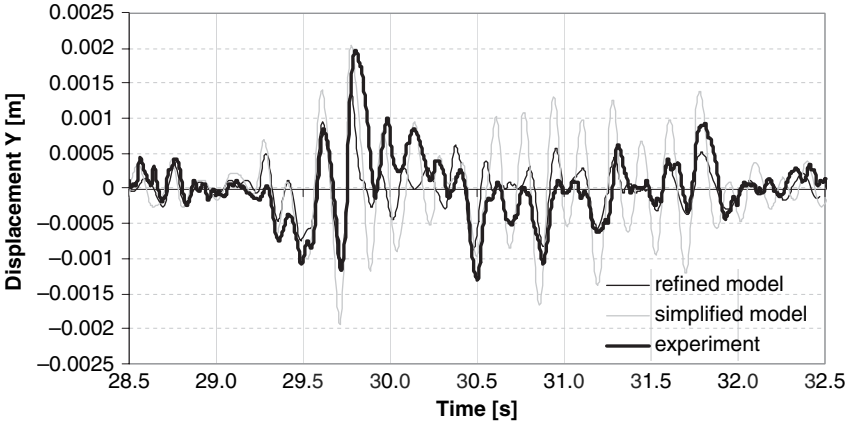


**FIGURE 15** Calculated and measured horizontal relative top Y displacement for the two models - Level T1.

Those results are intriguing, especially when considering the fact that for higher levels of loading (Fig. 19 – T6) the refined model reproduces more accurately the non linear behavior in the Y direction. One possible explanation could be that the shaking table responded in a non linear manner at T1, thus meaning that the assumption of linear elastic bars simulating the rods of the table should be abandoned (the axial stiffness of the vertical rods supporting the shaking table evolve during the seismic response). However, it is difficult to take into account this aspect, because the variation of the axial stiffness of the rods is not known in advance. For higher level of loading, this phenomenon becomes probably less important as compared to the nonlinear behavior of the specimen itself. Another possible explanation could be that the experimental behavior in the Y direction is certainly more complicated to simulate (shear forces in the Y wall, influence of the torsional behavior of the horizontal slabs, etc.)

Figures 16–19 compare the computed and experimental top displacements corresponding to the two last levels of loading. During T5 and T6, the specimen suffered from significant damage at the base, reinforcement bars buckled and at the end broke up (Figs. 7 and 8). The refined and simplified models give similar results in the X direction. The discrepancy in the Y direction is more important. Table 5 gives finally the maximum values of some variables obtained from the time history analysis for the highest level of loading (T6).

Complementary studies are obviously necessary to be able to take into account correctly the real behavior of the shaking table. However, as the mock-up responded mainly in the X direction (highest level of loading) where both modeling strategies reproduced correctly the behavior, they are used hereafter to highlight some important characteristics of the overall structural behavior.

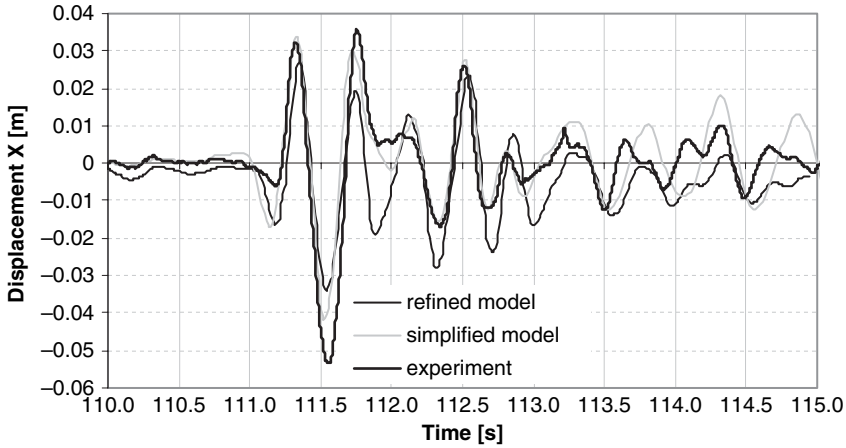


**FIGURE 16** Calculated and measured horizontal relative top X displacement for the two models - Level T5.

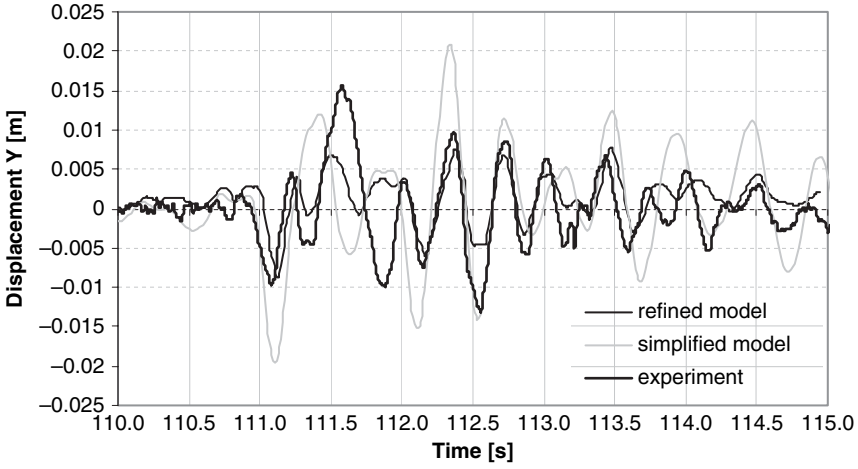


**FIGURE 17** Calculated and measured horizontal relative top Y displacement for the two models - Level T5.

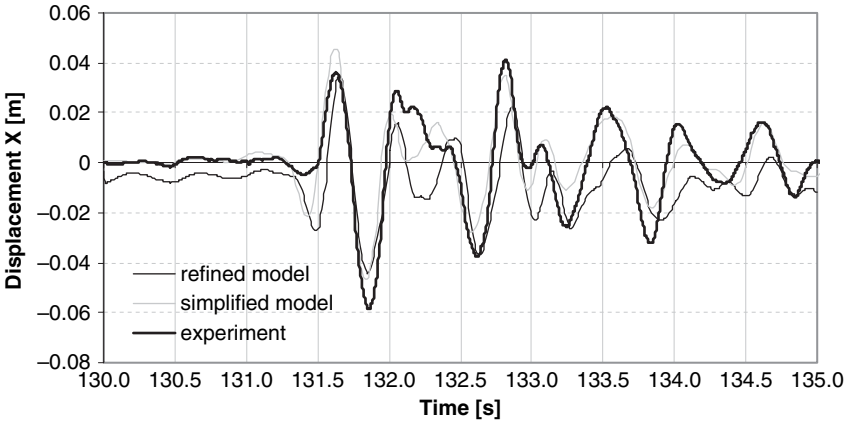


**FIGURE 18** Calculated and measured horizontal relative top X displacement for the two models - Level T6.

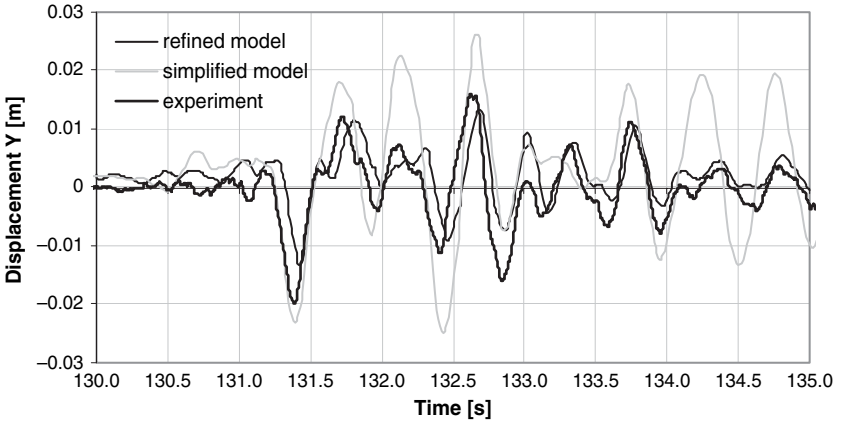


**FIGURE 19** Calculated and measured horizontal relative top Y displacement for the two models - Level T6.

### *6.2. Local Results*

Some local results obtained from the 3D refined dynamic analysis are presented in Fig. 20. This figure depicts the distribution of strains corresponding to the maximum top displacement attained in the X direction for the T5 applied motion. The results indicate that more damage is concentrated in the walls in the X direction than in those in the Y direction. Furthermore, important compressive strains are present at one end of the X wall, indicating that concrete may fail in this location due to excessive strains. This is in agreement with what was experimentally observed (even though from an earlier stage; Fig. 5): the concrete at wall extremities was heavily damaged due to compression and steel bars buckled or broke.

As mentioned before, previous experimental and numerical studies on lightly reinforced walls subjected to in-plane loading [Sollogoub *et al.*, 2000; Bisch and Coin, 2002; Kotronis *et al.*, 2005c) have underlined the importance of the variation of the dynamic

**TABLE 5** Maximum values - Level T6

| Test T6 | Refined model | Simplified model | Experiment |
|---|---|---|---|
| Relative top X displacement [mm] | 53.6 | 46.24 | 58.21 |
| Relative top Y displacement [mm] | 13.4 | 26.01 | 19.8 |
| Bending moment at the base - left wall [kN.m] | 249 | 245 | 299 |
| Bending moment at the base - right wall [kN.m] | 214 | 244 | 265 |
| Shear force at the base - left wall [kN] | 85 | 74 | 111 |
| Shear force at the base - right wall [kN] | 91 | 63 | 128 |
| Variation of axial force at the base, right wall [kN] | −224<br>+127 | −257<br>+126 | – |
| Variation of axial force at the base, left wall [kN] | −195<br>+132 | −314<br>+97 | – |

axial force. A first cause of this phenomenon is the extension mode due to bending: at maximum horizontal deflection the neutral axis is at its maximum distance from the center of the wall cross-section, the raising of masses is maximum and the dynamic variation of the axial force is a tensile force; the frequency of this vertical motion was found equal to two times that of the horizontal movement. The second reason of this phenomenon relies on the excitation of the natural vertical mode of the system: at cracks closure, when concrete recovers its stiffness, compression forces strongly increase and these shocks excite the vertical vibration mode of the system (shaking table + specimen).

It is to be emphasized that the variation of the axial force affects the value of the maximum bending moment, as these two parameters act together to determine the ultimate state of strain in the wall. Since the ECOLEADER specimen is subjected to bi-directional loading, the overturning moment perpendicular to the walls in the X direction induces a complementary compression axial force in one wall and a tensile axial force in the other. The total axial force variation in each X wall is then given by the superposition of the dynamic axial force due to the in-plane bending and of the axial force due to the out-of-plane loading. Figure 21 presents numerical results in terms of bending moment-axial force interaction diagrams at the base of the first story together with the variation of the axial load and moment. The values of the axial force and moment shown in this figure correspond at every time step of the seismic response, during the T5 input motion. This figure confirms the observed behavior and failure mode, since the limit states tend to be obtained with high axial force compression values.

Figures 22 and 23 show the relationship between stress and strain at the reinforcement at one edge at the base of an X wall. It can be seen that large incursions in the plastic range take place during the T4 input motion, while compression failure of the reinforcement is predicted for T5. It is thus clear that using an improved model for steel (as the one in Fig. 11) allows a better representation of the expected local behavior.

For the simplified model, the damage variables used in the uniaxial constitutive law for concrete (Fig. 13) vary between 0 (non damaged section) and 1.0 (completely damaged section). By filtering the values between 0.95 and 1.0 the micro-cracks are

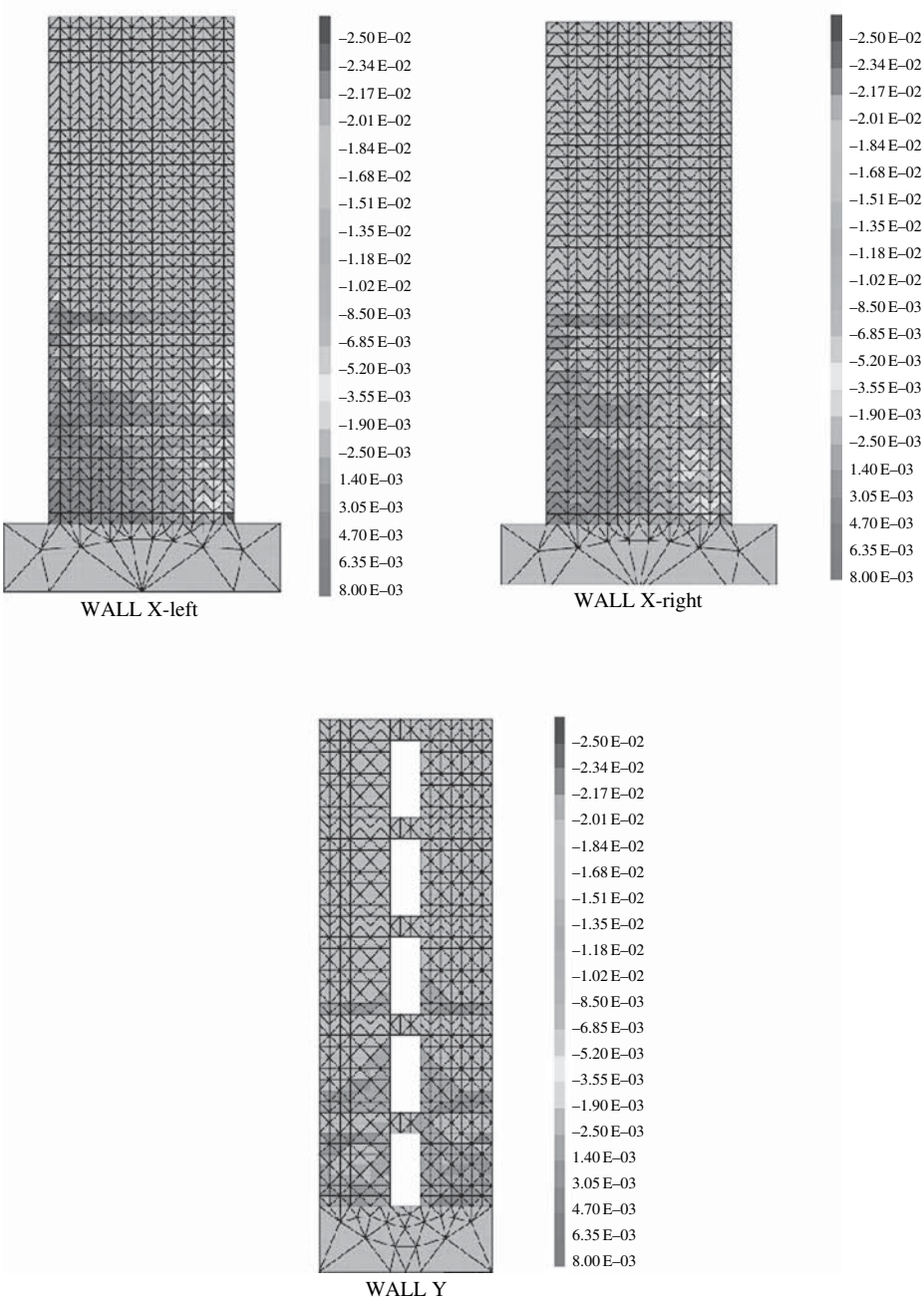


**FIGURE 20** Refined model: vertical concrete strain contours - Level T5.

omitted and one can have a picture of the visible cracks of the model (only points with damage between 0.95 and 1.0 are plotted). Figures 24 and 25 present the damage pattern due to tension at T6. As in the experiment, damage is concentrated at the base of the specimen and has significant values more in the X walls than in the Y one. Damage pattern due to compression is sketched in Fig. 26. Again, this figure is in accordance with

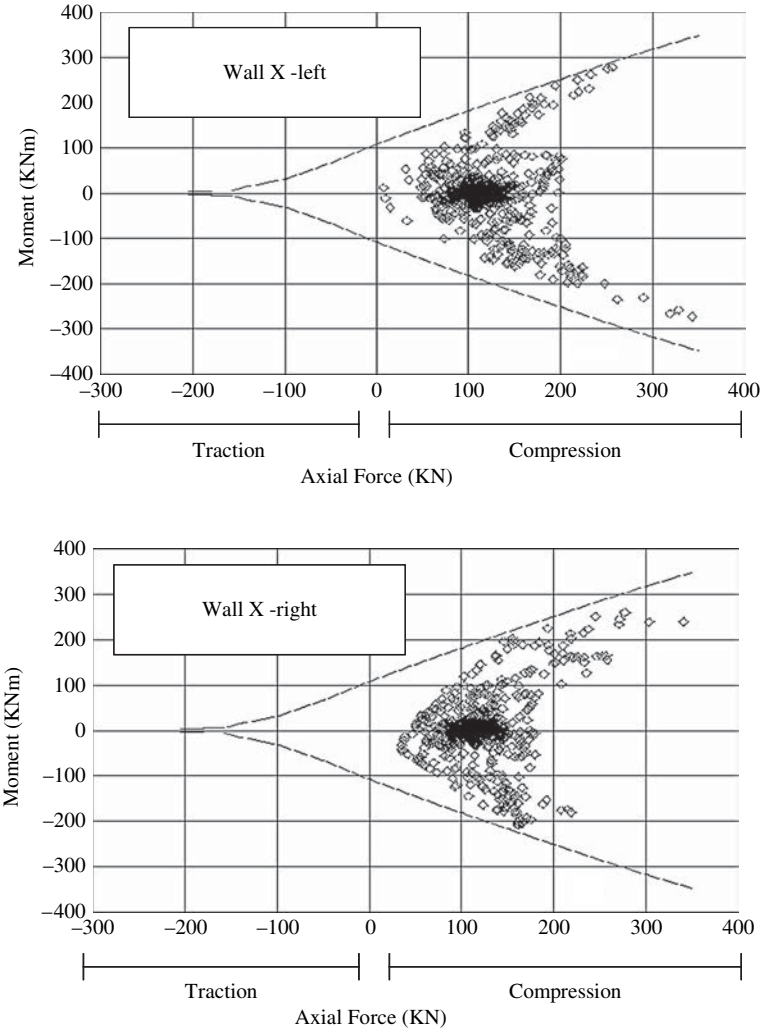


**FIGURE 21** Refined model: bending moment - axial force interaction diagrams and variation of the bending moment and axial force at the base of the first story - Level T5.

the experimental behavior of specimen with concrete being crushed at the base of both X walls under high compressive strains (Figs. 5, 8).

Although the constitutive relation used for steel is simpler, as compared to that of the refined model, one can have a clear indication of the local phenomena. Figure 27 shows the distribution of strain in reinforcement bars throughout the height of the specimen. At the base, strains are greater than 1.8%, value corresponding approximately to the ultimate strain measured experimentally. The multifiber model predicts rupture of the reinforcement bars at the T6 level, something also observed experimentally.

## 7. Parametric study: 3D loading

The main advantage of the multifiber model is that the number of degrees of freedom is relatively small allowing performing parametric studies. Hereafter, a new test sequence

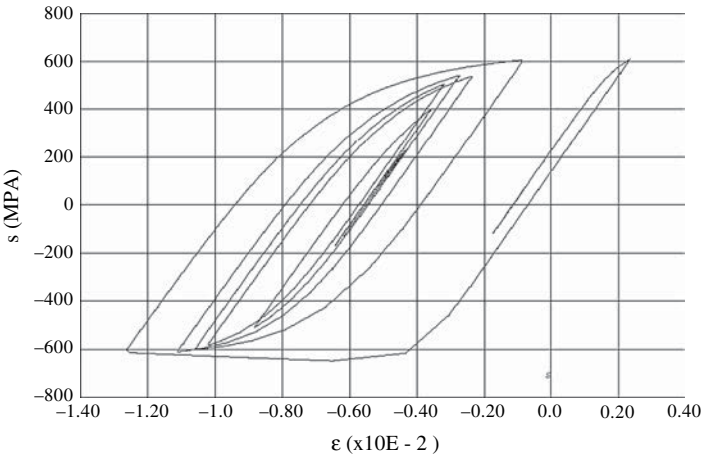


**FIGURE 22** Refined model: steel stress strain relationship - Level T4.

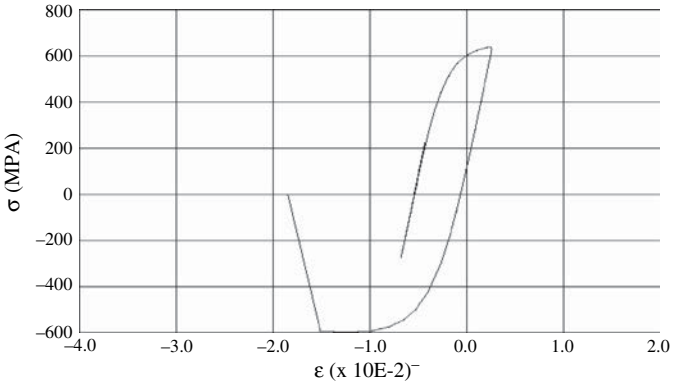


**FIGURE 23** Refined model: steel stress strain relationship - Level T5.

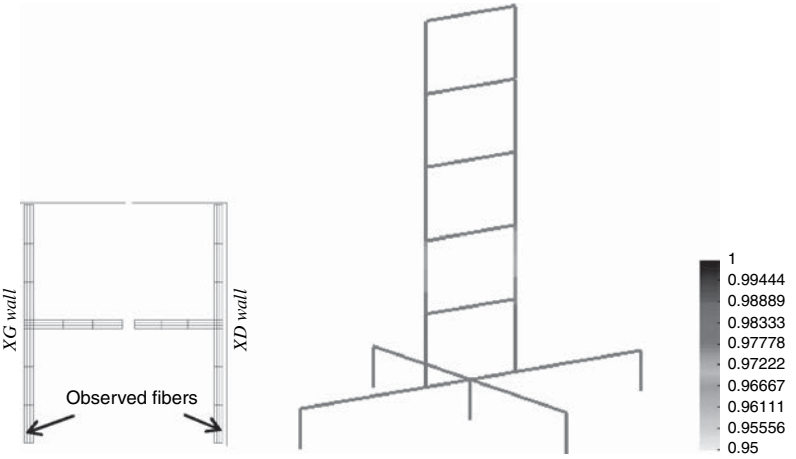


**FIGURE 24** Simplified model: distribution of damage due to tension - Level T6.

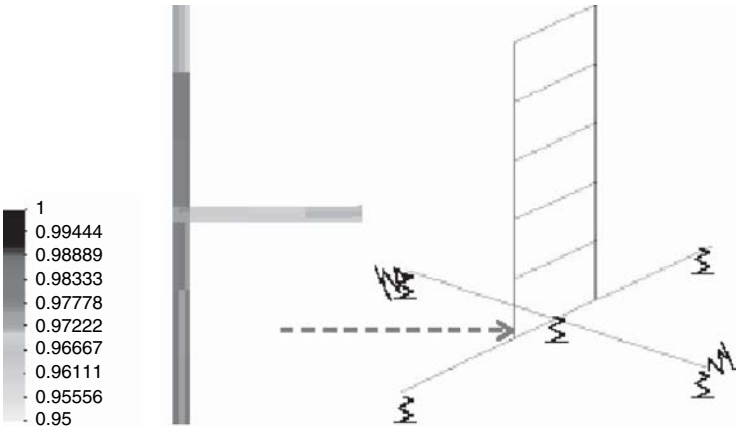


**FIGURE 25** Simplified model: distribution of damage due to tension at one section at the base - Level T6.

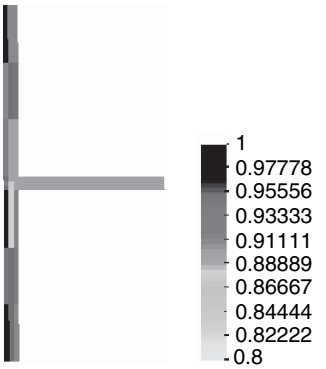


**FIGURE 26** Simplified model: distribution of damage due to compression in a T section at the base of the specimen - Level T6.

has been performed numerically (Table 6) in order to study the influence of a 3D earthquake (two horizontal and one vertical) loading on the behavior of the specimen.

The inter-story drifts predicted by the numerical model for the different sequences are shown in Fig. 28. The introduction of the second horizontal excitation clearly introduces an asymmetric behavior of the structure. Furthermore, the quantity more influenced by the loading conditions is the variation of the axial force (Fig. 29). The results show that a seismic load in the direction perpendicular to that of the walls increases the variation of the axial load by amplitude of the order of three (158,000 N is the static force at the base of a wall). Due to this effect, the walls could be subjected to a complete unload (even to a positive load, i.e., tension), or to a total vertical load equal to the double of the dead load.

Damage distribution is presented in Fig. 30 for two cases: B2 corresponds to the T6 level and B3 has an additional vertical direction of loading. In both cases, damage is concentrated at the base of the specimen. However, for the B3 case, a larger amplification of damage is observed certainly due to the increase of the amplitude of variation of the axial load (Fig. 29).

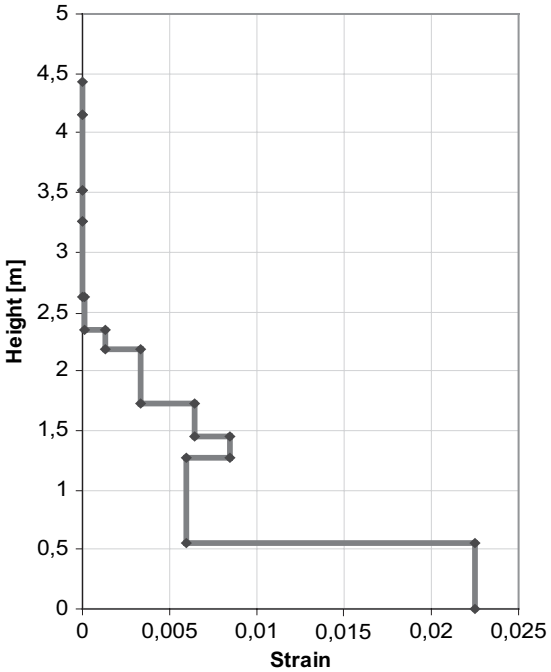


**FIGURE 27** Simplified model: strain of reinforcement at the XG wall - Level T6.

**TABLE 6** 3D loading: sequences of the numerical tests

| Tests | Direction X | Direction Y | Direction Z |
|---|---|---|---|
| A1 | 0.5g | – | – |
| A2 | 0.5g | 0.24g | – |
| A3 | 0.5g | 0.24g | 0.35g |
| B1 | 0.85g | – | – |
| B2 | 0.85g | 0.50g | – |
| B3 | 0.85g | 0.50g | 0.595g |

## 8. Conclusions

This work deals with the experimental and numerical campaign of a lightly reinforced concrete building tested on a shaking table (ECOLEADER program). The design of the specimen follows the minimal requirements for RC walls, as defined in the French and European codes (PS 92, EC8-1). The experimental campaign permitted to test the behavior of the specimen for increasing levels of loading sequences (varying from an almost elastic behavior till the appearance of significant damage in concrete and rupture of steel bars). During the T3 level—corresponding approximately to the design level—the specimen behaved as predicted by the design codes (horizontal cracks opened at the base of the X walls, where at each edge reinforcement bars buckled). The minimal requirements prescribed in the design codes are therefore verified. It is also noteworthy that the specimen was able to withstand higher levels of seismic loading and the failure mode was

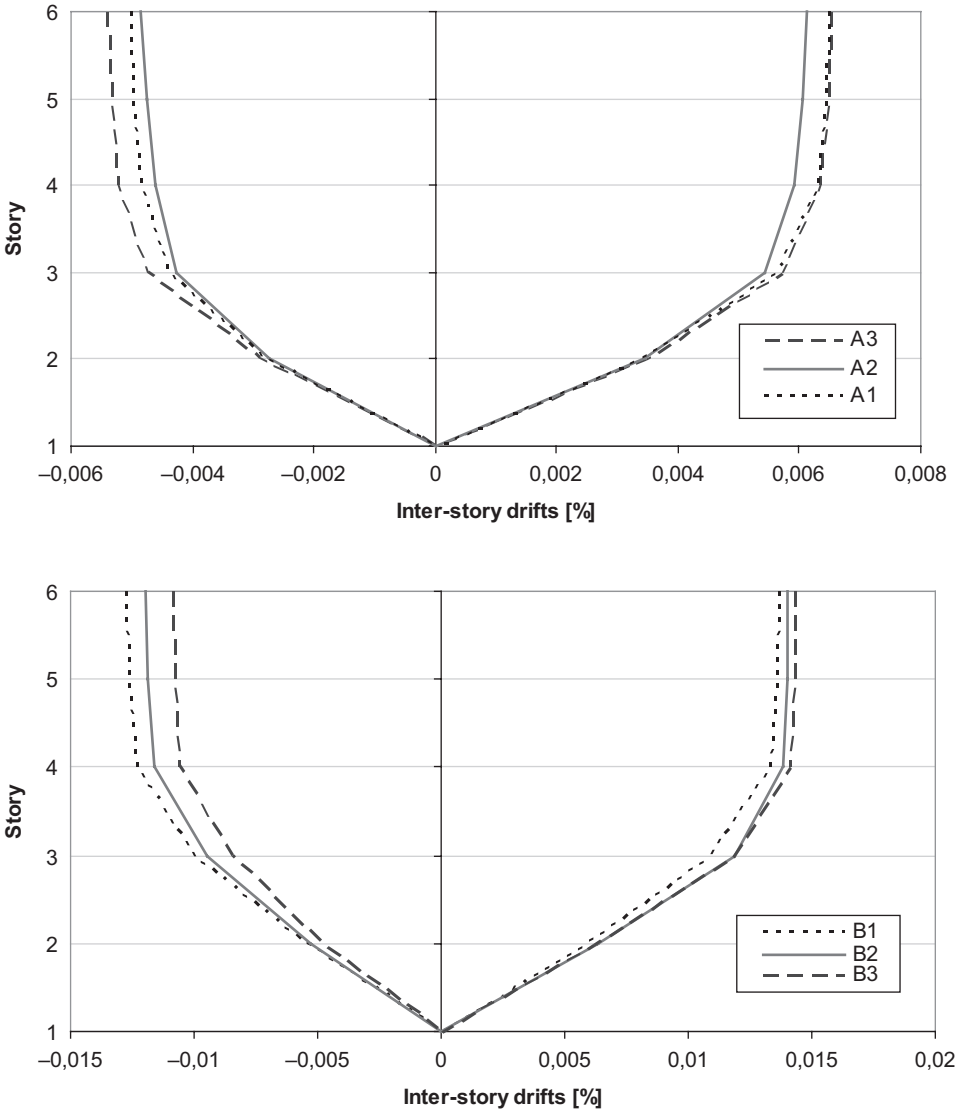


**FIGURE 28** Simplified model: 3D loading, inter-story drifts (XG wall).

still the one expected (spalling of concrete, broken reinforcement bars … Nevertheless, the mock up continued to resist with an overall rocking mechanism).

Two finite element strategies were also presented to simulate the nonlinear seismic response of the specimen: a refined one, using a 3D finite element mesh and a simplified one adopting a multifiber beam approach. The 3D finite element model requires a refined and realistic description of the wall geometry and reinforcement and detailed cyclic constitutive models for the materials. As compared to the multifiber approach, it is more time consuming, but it allows obtaining more precise detailed information at the global and local level. Its principal advantage lies in the fact that the mechanical properties of each constituent element of the wall are based on the actual local behavior of materials, and so the interaction between axial force, flexure and shear is directly taken

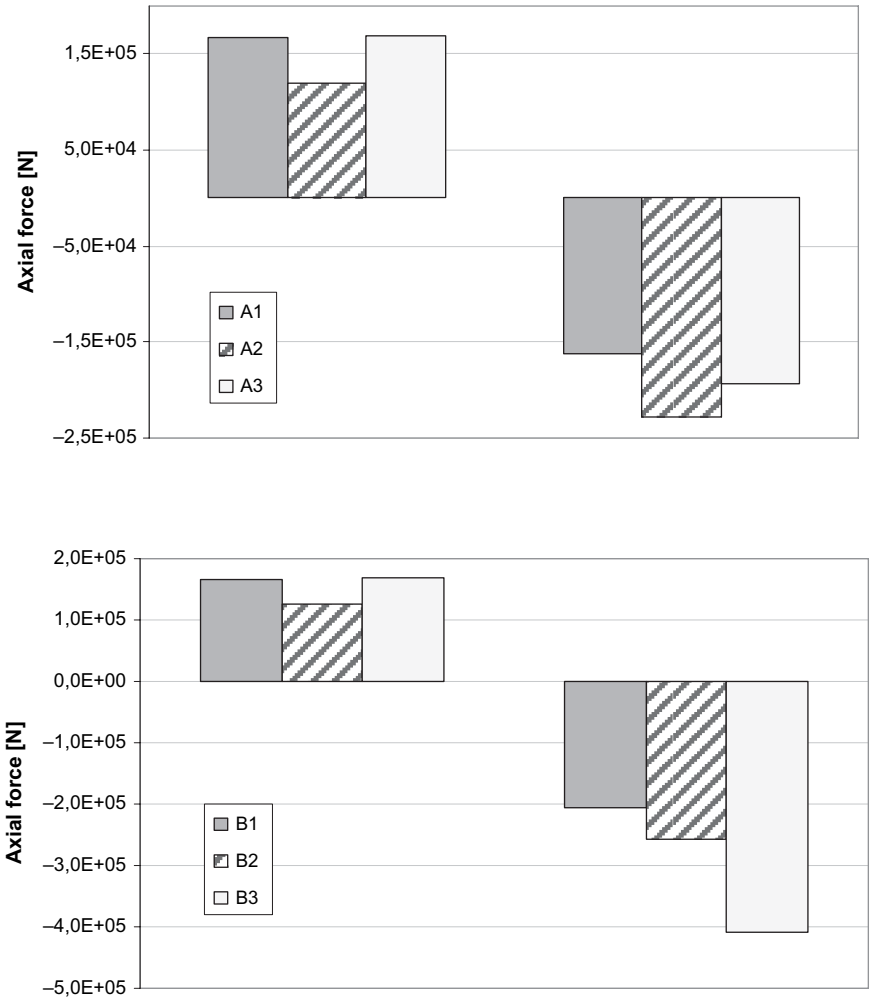


**FIGURE 29** Simplified model: 3D loading, variation of the axial load on the XG wall.

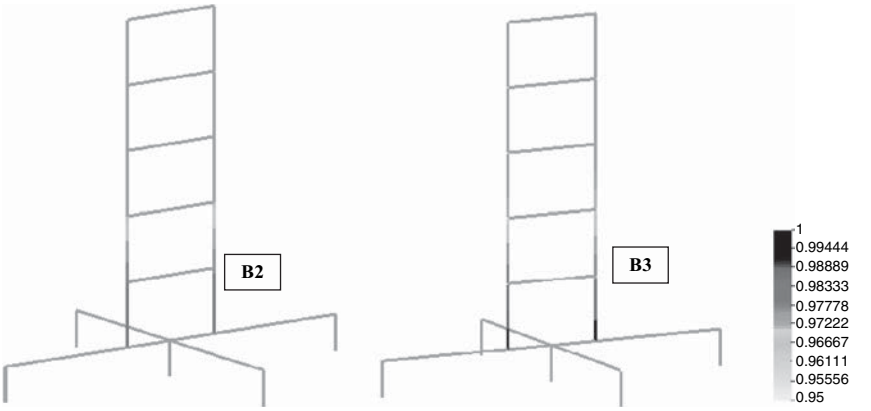


**FIGURE 30** Simplified model: 3D loading, distribution of damage due to tension.

into account. The simplified approach can perform fast computations, providing a sound understanding of the global behavior and taking into account with reasonable approximation local events, at quite low computational costs. It can be used to perform parametric studies and to test different cases such as the effect of different loading conditions or the mesh dependency. These features give indications about the integrated use of the two levels of analysis within the design verification procedures.

Nonlinear dynamic analysis proved to be a very powerful technique for animating and reproducing this ECOLEADER experimental program. The study revealed that the correct prediction of the experimental measurements depends not only on a good description of the cyclic non linear material behavior, but also on a proper modeling of the boundary conditions. Flexibility of the support mechanism needed to be considered and modeled since it is one of the important aspects in the dynamic behavior of the specimen. Since the variation of the axial stiffness of the rods was not known in advance, a linear elastic behavior was assumed for these elements. It was shown that this hypothesis may be responsible of the difference between the experimental and numerical results in terms of global response in the Y direction.

Nevertheless, both models were able to reproduce the global response in the X direction and to highlight the main aspects of the local behavior observed during the experiment. Damage due to tension but also due to compression was concentrated at the base of the X walls as in the real building. Buckling of the steel bars at the base of the X walls was reasonably predicted using a sophisticated constitutive relation for steel, although for a higher sequence of loading than that observed experimentally. Results have also identified the importance of the axial force variation for such lightly reinforced walls and its influence on the failure mode. This phenomenon can not be taken into account using a classical modal superposition or a pushover analysis. Finally, the parametric studies were able to give an indication about the amplitude of the variation of the axial load for a 3D earthquake loading, information that was not provided by the experimental program.

Such tools are necessary for engineers to improve design by introducing for example stronger confinement layout into the zones submitted to high compression stress. Furthermore, it seems that only nonlinear transient dynamic computations are able to evaluate accurately the margin of security for a given structure as they naturally take into account the variation of the axial load.

Nevertheless, it should be mentioned that none of the two strategies presented in this article consider bond-slip interaction between steel bars and concrete. Also, the localization of deformation could only be properly reproduced using an enhanced continuum theory, incorporating an internal length parameter to represent the meso-scale level [Pijaudier-Cabot and Bazant, 1987; Chambon *et al.*, 1998; Kotronis *et al.*, 2005a). Finally, the assumption of a constant damping matrix is clearly a limitation and needs further study [Ragueneau *et al.*, 2000].

## Acknowledgments

The authors would like to thank the European Community, the ECOLEADER consortium and the LNEC laboratory in Portugal for the experiments, la Fédération Française du Bâtiment (FFB) for providing the experts for the design of the French specimen and the French National Ministry for the Equipment (DRAST) for financing the numerical simulations. They are also grateful to A. Coin for his valuable advises that helped to improve the quality of the paper. They would finally like to thank the French research network RNVO for its financial support.

## References


ASTER finite element code official web site: http://www.code-aster.org.

Bisch, P. and Coin, A. [1994] "The CASSBA project," *Proc. of the 10th European Conference on Earthquake Engineering*, Vienna, Balkema, Rotterdam.

Bisch, P. and Coin, A. [1998] "The CAMUS Research," *Proc. of the 11th European Conference on Earthquake Engineering*, Paris, France, Vol. 2, pp. 1–13, Bisch, Ph. *et al.* Eds. Balkema Rotterdam.

Bisch, P. and Coin, A. [2002] "The CAMUS 2000 Research," *Proc. of the 12th European Conference on Earthquake Engineering*, London, September 9–13.

Bisch, P. and Coin, A. [2005] "Seismic behaviour of slightly reinforcement walls," *250th anniversary of the 1775 Lisbon earthquake - Proceedings*, Lisbon, Paper no 93, November 1–4, pp. 518–522.

Bisch, P. and Coin, A. [2006] "Comportement sismique des murs banchés," *Revue Européenne du génie civil*, **10/2**, 137–164.

Bisch, P. and Coin, A. [2007] "Seismic behaviour of slightly reinforced concrete walls: experiments and theoretical conclusions," *Bulletin of Earthquake Engineering*, **5**(1), 45–65.

Bisch, P, Coin, A, Ile, N, Kotronis, P., Mazars, J., Nguyen, X. H. and Reynouard J. M. [2007] "Performance sismique des structures à murs banchés: le programme européen ECOLEADER" *Revue Européenne de Génie Civil*, **11**(3), 311–353.

CAST3M finite element code official web site: http://www-cast3m.cea.fr/cast3m/index.jsp

Chambon, R., Caillerie, D. and El Hassan N. [1998] "One dimensional localisation studied with a second grade model," *European Journal of Mechanics A/Solids*, **17**(4), 637–656.

Chopra, A. K. [2000] *Dynamics of Structures: Theory and Applications to Earthquake Engineering,* 2nd ed. Prentice-Hall, Upper Saddle River, NJ.

Coin, A., Bisch, P. [2005] "Programme ECOLEADER. Rapport de fin de recherche," FFB et ZGF-BTM, 8 mars.

Coleman, J. and Spacone, E. [2001] "Localization Issues in Force-Based Frame Elements," *Journal of Structural Engineering*, **127**(11), 1257–1265.

Combescure, D. and Pegon P. [1994] "A fibre model accounting for transverse shear in CASTEM 2000," Special Publication No.I.94.59, pp.17, November, ELSA, Applied Mechanics Unit, Safety Technology Institute, European Commission, Joint Research Centre, Ispra, Italy.

Combescure, D., Queval, J. C., Chaudat, T. and Sollogoub, P. [2002] "Seismic behaviour of non symmetric R/C bearing walls specimen with torsion: experimental results and non-linear numerical modelling," *Proc. of the 12th European Conference on Earthquake Engineering*, London, U.K., Elsevier Ltd, September 9–13.

Dubé, J. F. [1997] "Modélisation multicouche des voiles en béton armé," *Revue française de génie civil*, **1**(2), 285–307.

Eurocode 8 [1995] Provisions for earthquake resistance of structures. Part 1–3: General rules – Specific rules for various materials and elements, CEN.

Eurocode 8 [2004] Design of structures for earthquake resistance. Part 1: General rules, seismic actions and rules for buildings, CEN, October.

Ghavamian, S. and Mazars, J. [1998] "Stratégie de calculs simplifiés pour l'analyse du comportement des structures en BA: le code EFICOS," *Revue française de génie civil*, **2**(1), 61–90.

Ghavamian, S., Davenne, L, and Gatuingt F. [2002] Elément de poutre multifiber (droite). Fascicule R3.08 - Document Code Aster.

Guedes, J., Pégon, P. and Pinto, A.V. [1994] "A Fiber/Timoshenko Beam Element in CASTEM 2000," Special Publication Nr. I.94.31, Applied Mechanics Unit, Safety Technology Institute, European Commission, Joint Research Centre, July, 55p, Ispra, Italy.

Ile, N. and Reynouard, J. M. [2000] "Non-linear analysis of reinforced concrete shear wall under earthquake loading," *Journal of Earthquake Engineering* **4**(2), 183–213.

Ile, N., Reynouard, J. M., and Georgin, J. F. [2002] "Non-linear response and modelling of RC walls subjected to seismic loading," *ISET Journal of Earthquake Technology*, **39**(1–2), 1–19.

Ile, N. and Reynouard, J. M. [2003] "Lightly reinforced walls subjected to multi-directional seismic excitations: interpretation of CAMUS 2000–1 dynamic tests," *ISET Journal of Earthquake Technology*, paper No. 435, **40**(2–4), 117–135.

Kotronis, P. [2000] "Cisaillement dynamique de murs en béton armé. Modèles simplifiés 2D et 3D," Ph.D., LMT, Ecole Normale Supérieure de Cachan, (http://tel.ccsd.cnrs.fr/).

Kotronis, P., Davenne, L., and Mazars, J. [2004] "Poutre 3D multifiber Timoshenko pour la modélisation des structures en béton armé soumises à des chargements sévères," *Revue Française de Génie Civil* **8**(2–3), 329–343.

Kotronis, P. and Mazars, J. [2005] "Simplified modelling strategies to simulate the dynamic behaviour of R/C walls," *Journal of Earthquake Engineering* **9**(2), 285–306.

Kotronis, P., Chambon, R., Mazars, J. and Collin F. [2005a] "Local second gradient models and damage mechanics: Application to concrete," *11th International Conference on Fracture*, Turin, Italy, Org. ICF, cd, paper no 5712, 20–25 March.

Kotronis, P., Mazars, J., Nguyen, X.H., Ile, N, Reynouard, J.M, Bisch, P and Coin, A. (2005b) "The seismic behaviour of reinforced concrete structural walls: Experiments and modeling," *250th anniversary of the 1755 Lisbon earthquake - Proceedings*, Lisbon, pp. 441–445, 86, 1–4 November.

Kotronis, P., Ragueneau, F., and Mazars J. (2005c) "A simplified modelling strategy for R/C walls satisfying PS92 and EC8 design," *Engineering Structures* **27**(8), 1197–1208.

La Borderie, C. L. [1991] "Phénomènes unilatéraux dans un matériau endommageable : modélisation et application à l'analyse des structures en béton," Ph.D. thesis, Université Paris 6.

Mazars, J. [1998] "French advanced research on structural walls: An overview on recent seismic programs," *Proc. of the 11th European Conference on Earthquake Engineering*, Opening lecture, Paris, France, Bisch, Ph. *et al*. Eds. Balkema Rotterdam, pp. 21–41.

Mazars, J., Kotronis, P., Ragueneau, F., and Casaux, G. [2006] "Using multifibre beams to account for shear and torsion. Applications to concrete structural elements," *Computer Methods in Applied Mechanics and Engineering*, **195**(52), 7264–7281.

Mazars, J., Nguyen, X.H., Kotronis, P., Ile, N., and Reynouard, J. M. [2005] "Etude sur le fonctionnement sismique de structures à murs à cellules contreventées," Contrat No.04MGC 5 07, Org. Rapport final (Novembre) - Contrat DRAST/ Mission Génie Civil, (http://hal.archives-ouvertes.fr).

Menegoto, M. and Pinto, P. [1973] "Method of analysis of cyclically loaded reinforced concrete plane frames including changes in geometry and non-elastic behaviour of elements under combined normal force and bending," *IABSE Symposium on resistance and ultimate deformability of structures acted on by well-defined repeated loads*, Final report, Lisbon, 328p.

Merabet, O. and Reynouard, J. M. [1999] "Formulation d'un modèle elasto-plastique fissurable pour le béton sous chargement cyclique," Contract Study EDF/DER, Final Report, No.1/943/002, URGC-Structures, National Institute for Applied Sciences, Lyon, 84 p.

Nguyen, X. H. [2006] "Vulnérabilité des structures en béton armé à voiles porteurs: expérimentation et modélisation," P.h.D thesis Institut National Polytechnique de Grenoble, juin (http://tel.ccsd.cnrs.fr/).

Nguyen, X. H., Mazars, J., Kotronis, P., Ile, N., and Reynouard, J. M. [2006] "Some aspects of local and global behaviour of RC structures submitted to earthquake - Experiments and modeling," *EURO-C 2006 Computational Modelling of Concrete Structures* Meschke, G., de Borst, R., Mang, H., Bicanic, N. Eds. 27th-30th March, Mayrhofen, Tyrol, Austria pp 757–766.

Papaioannou, I., Fragiadakis, M., and Papadrakakis, M. [2005] "Inelastic analysis of framed structures using the fiber approach," *Proc. of the 5th International Congress on Computational Mechanics (5th GRACM)*, Limassol, 29 June – 1 July.

Petrangeli, M., Pinto, P. E. and Ciampi, V. [1999] "Fiber element for cyclic bending and shear of RC structures. I: theory," *Journal of Engineering Mechanics*, **125**(9), 994–1001.

Pijaudier-Cabot, G. and Bazant, Z. P. [1987] "Nonlocal damage theory," *Journal of Engineering Mechanics* ASCE, **113**, 1512–1533.

Proix, J. M., Laurent, N., Hemon, P., and Bertrand, G. [2000] "Code Aster, manuel de référence. Fascicule R3.08: Eléments mécaniques à fibre moyenne," Document: R3.08.03. Calcul des caractéristiques d'une poutre de section transversale quelconque.

PS92 [1995] Règles de construction parasismique, Règles PS applicables aux bâtiments, dites Règles PS92. Norme française, AFNOR, 217p.

Ragueneau, F., La Borderie, Ch., and Mazars, J. [2000] "Damage model for concrete like materials coupling cracking and friction, contribution towards structural damping: first uniaxial application," *Mechanics Cohesive Frictional Materials*, **5**, 607–625.

Sollogoub, P., Combescure, D., Queval, J-C., and Chaudat, T. [2000] "In Plane Seismic Behaviour of Several 1/3rd Scaled R/C Bearing Walls – Testing and Interpretation Using Non-Linear Numerical Modelling," *Proc. of the 12th World Conference on Earthquake Engineering*, Auckland, New Zealand, cd-rom.

Spacone, E., Filippou, F. C., and Taucer, F. F. [1996] "Fiber beam-column model for nonlinear analysis of R/C frames. I: formulation," *Earthquake Engineering and Structural Dynamics* **25**(7), 711–725.

Taucer, F., Spacone, E, and Filippou, F.C. [1991] "A fiber beam-column element for seismic response analysis of reinforced concrete structures," Report No. UCB/EERC-91/17, University of California, Berkeley.